Mechanical Development of a Very Non-standard Patch Array Antenna for Extreme Environments

Richard Hughes, Neil Chamberlain, Julie Jakoboski, Mihail Petkov
Jet Propulsion Laboratory
California Institute of Technology
4800 Oak Grove Drive
Pasadena, CA 91505
818-354-4209
Richard.C.Hughes@jpl.nasa.gov

Abstract—This paper describes the mechanical development of patch antenna arrays for the Juno mission. The patch arrays are part of a six-frequency microwave radiometer instrument that will be used to measure thermal emissions from Jupiter. The very harsh environmental conditions in Jupiter orbit, as well as a demanding launch environment, resulted in a design that departs radically from conventional printed circuit patch antennas. The paper discusses the development and qualification of the Juno patch array antennas, with emphasis on the materials approach that was devised to mitigate the effects of electron charging in Jupiter orbit.

TABLE OF CONTENTS

1. INTRODUCTION 1
2. ANTENNA REQUIREMENTS 2
3. DESIGN AND MATERIAL SELECTION 3
4. PROCESS DEVELOPMENT AND VERIFICATION 4
5. METAL PATCH DEVELOPMENT 10
6. ANTENNA SUBSYSTEM TEST AND VERIFICATION 13
7. SUMMARY 14
8. REFERENCES 15
9. BIOGRAPHIES 16
10. ACKNOWLEDGMENTS 16

1. INTRODUCTION

Juno is a New Frontiers mission with the principal goal of understanding the origin and evolution of Jupiter [3]. The Juno spacecraft, which was launched in August of 2011, has a scientific payload comprising 7 instruments, one of which is a microwave radiometer (MWR). This paper describes the development of two of the antennas associated with the MWR instrument, and in particular the unconventional design approach that was devised for these antennas to meet the extreme radiation environment in the vicinity of Jupiter.

The MWR instrument comprises 6 radiometer receivers with 6 separate antennas ranging in frequency from 600 MHz to 22 GHz [2]. The instrument requires antennas with low sidelobes to minimize interference from synchrotron radiation (generated by high-energy electrons trapped in Jupiter's radiation belts) and with low loss. Additionally, the antennas have very demanding environmental requirements, including robustness to withstand high dynamic launch loads, a wide protoflight temperature range of -135°C to +120°C, and exposure to radiation and high-energy electron flux [1].

For low loss RF performance in an electron charging environment, an all-metallic antenna is the first choice. When the MWR instrument was originally proposed in the Juno Concept Study Report, an aluminum corrugated horn was selected for the highest frequency antenna (A6 at 22 GHz) and aluminum slotted waveguide antennas were selected for the other frequencies (A1 at 600 MHz, A2 at 1.25 GHz, A3 at 2.6 GHz, A4 at 5.2 GHz, and A5 at 10 GHz) [10]. However, as studies progressed through Phase A of the mission, it became clear that slotted waveguide antennas would not be practical for the two lowest frequency antennas, A1 and A2, while at the same time meeting volume and mass requirements. The A1 antenna measures 1.6 m by 1.6 m and takes up an entire face of the hexagonal Juno spacecraft. The original mass allocation for the 6 MWR antennas was 20.7 kg, which was a very aggressive goal (the ensemble of flown MWR antennas has a mass of 33.5 kg; the largest slot array, A3, weighs 7.25 kg).

This pushed the design of the A1 and A2 antennas toward corporate fed patch arrays. Patch antennas normally use multilayer printed circuit technology to form both the patches and the feed network in the form of etched metallic traces. This is not desirable because printed circuit technology uses a lot of dielectric that would be susceptible to bulk electron charging in the Jupiter environment. To deal with this problem, an antenna architecture and materials approach was developed that would a) separate the functions of the patch radiator and corporate feed network, b) minimize the overall dielectric content of these components, and c) modify/select the dielectric materials that are used in order to mitigate against the effects of electron charging.

To this end, the antennas were configured as 5x5 arrays of patch elements mounted on one side of the panel, fed by a corporate network of power dividers/combiners (to effect the desired sidelobe levels) and coaxial cables mounted on the opposite side of the panel [5]. Initially the 25 patch

978-1-4577-0557-1/12/$26.00 ©2012 IEEE

elements were supported on Astroquartz honeycomb pedestals that were doped with carbon to bleed off impacting electrons. The patch elements also had a ground wire attached at the center to panel ground to help bleed accumulated charge on the patch itself. The power dividers/combiners were configured as 5-way air stripline circuits on thin printed circuit boards suspended in lightweight aluminum housings. While the power divider/combiners would be shielded somewhat from the electron flux by the aluminum honeycomb panel and aluminum housing, it was later found to be necessary to coat the stripline circuit board with germanium to bleed off residual electrons that might penetrate the panel and power divider/combiner housing. The coaxial cables and connectors, which provide the means of interconnecting power dividers/combiners and patch elements, were constructed with a silicon dioxide foam dielectric inside a stainless steel jacket, making them resilient (but not impervious) to the effects of electron charging. This selection of materials, while driven principally by environmental requirements, also resulted in low RF losses (about 1dB) and good impedance bandwidth (approximately 9%). Figure 1 illustrates the resulting antenna architecture and Figure 2 illustrates the initial antenna cross section showing patch, feed and interconnect.

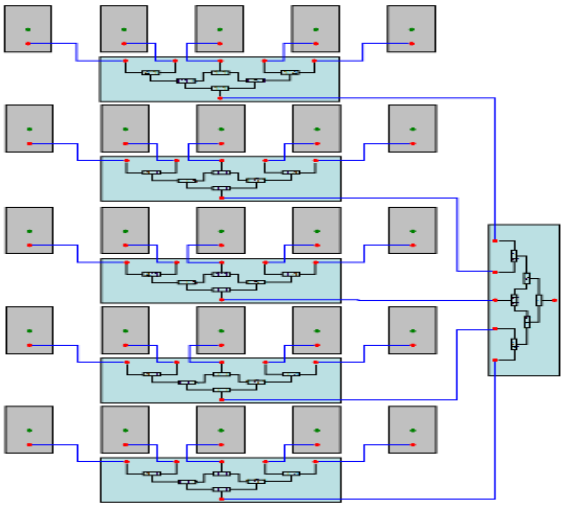

Figure 1. Antenna architecture.

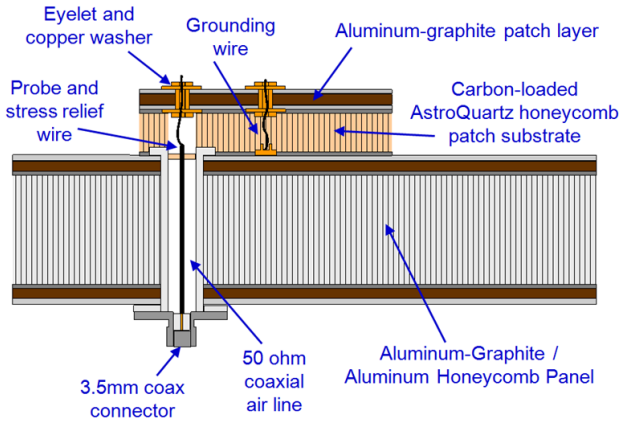

Figure 2. Antenna element cross-section, initial design.

2. Antenna Requirements

The Jupiter environment for the large MWR antennas was extremely demanding [4]. Starting with launch, the acoustic loading for the Atlas V 551 launch vehicle was relatively high with an overall sound pressure level (SPL) of 140.3 dB. As a result the random vibration levels for the power dividers/combiners attached to the large A1 antenna panel were extremely high, initially starting out at 60.1 grms protoflight and finally settling to 40.6 grms protoflight. At Jupiter, the antenna operating temperatures were very low (starting at -200°C protoflight before finally settling at -135°C).

Shortly after launch when the fairing had separated, the Atlas V launch vehicle went into a transfer orbit, causing the antennas to be heated from free molecular heating and solar loading. The antennas were designed to a relatively high protoflight maximum temperature of 120°C to withstand this heat loading, but requirements ended up being levied on the launch vehicle in order to prevent the antennas from exceeding their maximum allowable flight temperature of 100°C. Specifically, the steady-state solar flux on MWR A1 and A2 could not exceed 450 W/m^2 (allowing spin-averaging of up to 2 minutes), and the transient direct solar exposure could not exceed 1370 W/m^2 over a 13 minute interval. These requirements are based on an initial antenna temperature of 21°C or less. Without these requirements, the patch temperature would have risen to over 300°C in the presence of direct solar exposure at 1370 W/m^2, and this would have exceeded the capability of the adhesives used to attach the patches.

The Juno orbit is highly elliptical to minimize radiation exposure, but the levels are still very high; so high in fact that most of the electronics are housed in a titanium vault. The Juno internal electrostatic discharge (IESD) environment was determined by estimating the temporal variations in flux density (due to solar storms) at 10 times the spatial average, at a baseline electron energy of 1 MeV. The flux more or less increases with the number of orbits, but for MWR (which is required to operate through orbit 10), the peak flux is 16 pA/cm^2. Toward the end of the 34 orbit mission life, the peak flux levels are 3 to 4 times higher; a factor of about 2-3 times larger than the environment for Galileo. At the back of the panel, where coaxial cables and power divider/combiner assemblies are located, the flux density was estimated to be 4 pA/ cm^2. The antenna panel, roughly speaking, reduces the incident flux by a factor of 4. Mechanical and environmental requirements are summarized in Table 1.

Micrometeoroid fluence was also taken into account during the design of the MWR antennas. The fluence (a measure of spatial density of particles a given mass and velocity) for a micrometeoroid of greater than 1 g traveling at a speed of 10 km/s is about 10^{-6} m^{-2}. Analysis showed that the probability of penetrating a cable sheath or power divider/combiner

casing for the A1 and A2 antennas was less than 0.5% and it is by no means certain that breaching the shielding of an element of the feed network would result in a failure. The probability of puncturing a patch in the original design (Figure 2) of the A1 antenna was about 1% over the lifetime of the mission. However, separate RF analysis showed the patch element to be very robust with respect to small punctures, even in some instances to punctures that resulted in a short to ground. The metal patches developed later in are even more resilient to micrometeoroids.

Table 1. Mechanical and environmental design requirements.

Description	Unit	A1	A2
Protoflight Temp	°C	-135 to +120	
Flight Allowable Temp	°C	-120 to +100	
Vibration/Acoustic	grms	40.6	23.5
Electron Flux @ 1MeV	pA/cm^2	≤ 16	
Steady State Solar Flux	W/m^2	≤ 450	
Transient Solar Flux	W/m^2	≤ 1370	
Mass	kg	≤ 14	≤ 5
Area	cmxcm	160x160	77x77
Depth	cm	15	12

Table 2. RF design requirements.

Description	Unit	A1	A2
Center Frequency	MHz	600	1250
Bandwidth	%	≥ 4.5	
3dB Beamwidth	deg	≤ 22	
Average Sidelobe			
$25° < \theta \leq 32°$	dB	≤ -24	
$32° < \theta \leq 40°$	dB	≤ -28	≤ -27
$40° < \theta \leq 70°$	dB	≤ -35	≤ -34
$70° < \theta \leq 100°$	dB	≤ -43	≤ -42
$100° < \theta \leq 150°$	dB	≤ -44	≤ -43
$150° < \theta \leq 180°$	dB	≤ -40	
Avg Return Loss	dB	≥ 15	
Insertion Loss	dB	≤ 1.65	≤ 1.75
Pointing Accuracy	mrad	≤ 9	
Polarization		linear	

RF requirements are summarized in Table 2. The key driving RF requirement was the antenna pattern sidelobe level and low uncertainty in the analysis/measurement of the level. The sidelobe requirement is based on the average total power over an annulus in the antenna pattern. Low sidelobes are necessary to suppress synchrotron emissions when the antenna main beam is pointing toward the planet. Sidelobe performance heavily influenced the power divider/combiner design. The bandwidth of the antenna array was driven by the patch element, as the feed network is relatively broadband. The patch bandwidth is determined primarily by the height of the patch as well as the dielectric constant of the supporting substrate.

3. Design and Material Selection

The MWR patch array antennas can be viewed as an assembly of three major components: 1) a support panel on which is mounted 2) an array of patch elements on one side that are connected (by means of feed-throughs in the panel) to 3) a feed network on the opposite side of the panel. For the MWR patch antennas, the biggest problem turned out to be the high flux of high energy electrons that could produce bulk charging of dielectric materials on the patch side of the antenna, even through thin layers of metallic shielding provided by the patch material. The use of dielectric materials on the feed side of the antenna was a concern, but less of a problem owing to the shielding afforded by the structural panel, steel cable jacketing, and aluminum power divider/combiner housing.

The design of the honeycomb support panel was relatively standard, using thin (0.25mm) quasi-isotropic graphite composite (M55J/cyanate-ester) facesheets, with a co-cured aluminum foil outer layer, sandwiching a lightweight aluminum honeycomb core. The aluminum outer layer acted as an antenna ground plane and provided a low emissivity surface to reduce heat loss in the Jupiter environment. The panel main attachments to the spacecraft at 4 locations were either a pattern of 4 large inserts in a higher density core and a facesheet doubler (used for 2 of the A1 and for all 4 of the A2 attachments) or edge clips using an aluminum block and graphite composite facesheet doublers (for 2 of the A1 attachments).

Because of the large number (49) of power divider/combiner and semi-rigid cable attachment points on the honeycomb panel, we did not use the more standard potted metallic inserts. Instead, we opted to use the much lighter, bonded-on, Click Bond™ surface-mount fittings that consist of an A-286 metallic stud attached to a graphite composite base plate. This approach was very successful because they required less adhesive, were easy to install, and provided an acceptable load capability after thermal cycling of 980 N minimum in tension and 1940 N minimum in shear. These studs were electrically grounded to the support panel by means of a small bead of conductive epoxy.

Many antenna materials, such as metals and some polymerics such as epoxies and cyanate-esters, are reasonably radiation tolerant; however common RF materials, such as Teflon, were not allowed in the Juno environment for our application [7]. The prohibition of Teflon drove us to use coaxial cables for the feed network with dielectric insulator made of silicon dioxide foam. This material has much better radiation performance while at the same time providing excellent RF loss. On the patch side, a thick, low-permittivity dielectric substrate was necessary to provide the required RF bandwidth. This property, in tandem with the need to minimize mass, resulted in the selection of Astroquartz honeycomb as the patch substrate. In order to bleed off the electrons deposited inside

dielectrics, the materials had to have a volume resistivity $\leq 10^{12}$ Ω cm. For the Astroquartz honeycomb material and attachment adhesives, we tried a standard industry approach [11] of carbon loading the cyanate-ester material to provide high resistivity bleed paths for the charge build up. JPL went through an extensive development process with industry partners to manufacture carbon-loaded dielectric materials that had the required properties, namely bulk resistivity, structural/adhesive performance, and RF performance.

During the course of this development, we experienced considerable difficulty in producing materials that would have the necessary environmental and RF performance. This is due to the counteracting nature of the different requirements. To underscore this crucial finding, consider the RF losses in the patch, which are minimized by having low conductivity (i.e., low carbon loading) and low loss tangent in the substrate materials. However, to obtain the required volume resistivity, a high loading of carbon is required in both the honeycomb and adhesives. Furthermore, the high carbon loading diminishes the strength of the adhesives, resulting in poor bonding (and ultimately delamination) over the large Juno protoflight temperature range. We finally concluded that carbon loading could not adequately meet the IESD, structural, and RF requirements simultaneously.

This ultimately led to the development of an all-metallic antenna element that eliminated dielectric from the patch construction and thereby obviated all issues relating to IESD [6]. However, the remainder of the antenna, including the panel and feed network, was implemented as originally conceived at the end of Phase B, with the relatively minor design changes of 1) coating the thin power divider/combiner circuit boards with germanium to provide acceptable IESD performance, and 2) increasing the core density of the aluminum honeycomb support panel for the A1 antenna to provide acceptable structural margins.

In the remainder of this paper, we discuss the process by which the materials, components, and assemblies were developed and verified, including the feed network and the carbon-loaded patch that was later abandoned.

4. Process Development and Verification

This Section discusses the efforts that were undertaken at JPL to develop and qualify materials and components for the Juno MWR patch array antennas. There were three main parts to this effort focusing on 1) the patch elements, 2) the components of the feed network and 3) the support panel.

4.1 Patch Element

A common approach to preventing electrostatic discharges due to bulk electron charging in plastics is to carbon load the material to provide low conductivity self-discharge paths [12]. However, carbon loading does introduce undesirable RF losses [13] and a reduction in the mechanical strength and adhesive properties [12]. Therefore it is desirable to use the lowest carbon loading that meets the self-discharge volume resistivity of $\leq 10^{12}$ Ω cm, with some margin.

The process for developing carbon-loaded materials for the patch element substrates was perhaps one of the most challenging aspects to developing the MWR instrument hardware. The process starts by ordering sheets of carbon impregnated prepregs and film adhesives from a select list of vendors. These materials are then subjected to a variety of tests. First, it is necessary to assess the bulk conductivity of the materials. Initially, this was done by making DC conductivity measurements with a high resistance ohm-meter. However, this technique was later found to be inaccurate, and we later relied on a much more elaborate vacuum electron charging technique. Second, once acceptable conductivity was obtained, the materials were assessed for RF loss and permittivity. This was done by making RF measurements in a cavity resonator. With acceptable raw materials, the carbon-loaded Astroquartz honeycomb could be ordered.

When the carbon-loaded honeycomb and film adhesives became available, it would be necessary to prepare coupons for a second round of testing. Coupons of the adhesive and adhesive / honeycomb composite were prepared to do flat-wise tensile testing. Some of these coupons were thermal cycled. Coupons were also prepared to do vacuum electron charging measurements, to verify that the carbon-loaded honeycomb had the required discharge characteristic. A second round of RF permittivity and loss tangent measurements were made on the adhesive-honeycomb substrate. This last step is necessary not only to verify acceptable RF losses within the patch, but also to ascertain the dielectric constant in order to accurately tune the patch element. As an unfortunate but necessary consequence of the process, if any one of the required performance metrics is off, bulk conductivity, bonding strength, or RF loss, then whole process must be repeated.

For the Juno project our intention was not to evolve the state of the art in carbon loading but was rather to use standard industry processes that could be used to provide the quantities of material needed to manufacture the A1 and A2 antennas. To this end we chose to work with two composite industry suppliers of cyanate-ester prepregs and adhesives using their standard carbon materials and mixing processes. The first attempts involved a very high conductivity carbon black (Cabot BP2000) that potentially would allow very low percent loading to minimize effects on the mechanical properties. The cyanate-ester polymer was cast into approximately five 30 cm x 30 cm sheets 2 to 3 mm thick with BP2000 carbon loadings of 0.75%, 0.58%, 0.38%, 0.20% and 0.10% by weight respectively. These samples were tested for volume resistivity and for RF complex permittivity the results of which are presented in Figure 3.

Extrapolating the results of bulk polymer samples to that of a matrix material in an Astroquartz honeycomb indicated

that a bulk loss-factor much above 0.1 would result in unacceptable RF losses. The initial volume resistivity measurements indicated acceptable resistivity in all the various loading levels but in hindsight we realize that the measurements were suspect and were likely affected by surface contaminants such as mold release for the cast samples. In any event a test production run of cyanate-ester and Astroquartz honeycomb with 0.20% BP2000 carbon loading was procured. Although the RF loss factor was close to that predicted from our coupon tests, there was no measureable conductivity.

On the advice of our prepreg vendors we then switched our attention to a lower conductivity "acetylene black" carbon that they were then using for other customers for similar applications. After testing prepreg samples of cyanate-ester Astroquartz prepreg with low-conductivity carbon loadings of 4% and 2% and high-conductivity carbon loading of 0.3% and 0.2%, we procured Astroquartz honeycomb with a 4% of low-conductivity carbon loading.

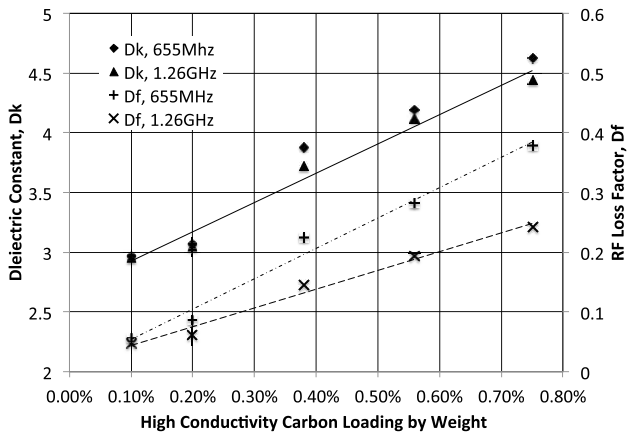

Figure 3. Cyanate-ester polymer dielectric constant and RF loss factor versus BP2000 carbon loading level.

For the cyanate-ester film adhesive used to attach the patch Astroquartz honeycomb to the aluminum foil covered patch and panel, we started with test samples of a 6% carbon loading and later evaluated a range of carbon loadings down to 2%. Following some early adhesive failures during thermal cycling with Astroquartz honeycomb bonded to panel facesheet material using a 5% carbon loaded film adhesive, a series of mechanical tests of available materials was performed which are summarized in Table 3. During the testing it was established that the addition of a silane primer (Z6020) significantly improved cyanate-ester adhesion to aluminum, so later tests used this primer.

Table 3. Astroquartz honeycomb to facesheet flatwise tensile testing.

Adhesive Carbon Loading	Honeycomb Carbon Loading	Thermal Cycling (psi)	10 cycles: +120C to -135C (psi)	10 cycles: +130C to -150C (psi)	Adhesive Failure Location
2.0%	0.2% BP2000	183.7	152.5	134.5	Honeycomb
2.5%	4% Acetalene Black		290.3		Honeycomb
3.0%	4% Acetalene Black		270.2		Honeycomb
4.0%	4% Acetalene Black		288.0		Honeycomb
5.0%	0.2% BP2000	89.1	0.0*		Aluminum
6.0%	none	143.9			Honeycomb

* Adhesive failure occurred at aluminum foil interface

The limited data indicate some possible trends:

- Except for the bond failure of the 5% carbon-loading sample at the aluminum foil that is attached to the graphite composite face sheet, all other tests failed at the adhesive to honeycomb bond.
- Adhesive bond strength to the 0.2% BP2000 loaded Astroquartz honeycomb is significantly lower than for no loading or 4% acetylene black loading, but the reason why was not further investigated.
- Bond strength is degraded by deep thermal cycling.
- Bond strength appears to degrade at high carbon loading levels but the 5% loaded material appears to have unusually low bond strength and may have had some process variability issues.

The most problematic issue in evaluating carbon-loaded materials that we experienced was the difficulty in making reliable volume resistivity measurements when dealing with thin sheets of material such as film adhesives and Astroquartz prepregs. For film adhesives we used a through thickness resistance measurement with conductors bonded to each side of the cured adhesive. This showed a lot of sample-to-sample variability at low carbon loadings because the presence or absence of a few carbon chains bridging the two conductors could make a big difference in the measured resistance. Although the average conductivity over many samples may be within an acceptable range the isolated nature of conducting chains did create non-conducting regions that could charge to high voltages. For Astroquartz prepregs we made measurements along the plane of the sheets, which were cured with conductors bonded to opposite edges. For this material at low carbon loading levels the resulting high resistances became susceptible to moisture absorption, surface contamination and parallel conduction paths through the air.

To resolve the uncertainty in the resistivity measurements, cured samples of the adhesive and the Astroquartz

honeycomb were exposed in vacuum to a 30keV, 1nA/cm^2 electron flux and monitored for charge build up, generation of electric arcing and rates of self-discharge. Unfortunately samples for all carbon loading levels developed high voltage regions and exhibited periodic arcing although the period between arcing increased significantly as carbon loading level increased.

The fabrication of charge dissipative epoxy by carbon addition is inherently difficult due to the poor control over the carbon dispersion within the material. Evidence for carbon clustering was obtained by SEM examination (Figure 4). To minimize the static surface charging from the electron beam, SEM images were taken near the zero-point energy determined by using the high-energy (Duane-Hunt) limit in the x-ray spectrum [14][15]. At that energy, the balance of incident and outgoing (secondary and backscattered) electrons is zero, and local differences in conductivity due to conductive paths formed by sub-surface carbon clusters result in local differences in surface potential. Such areas (dark spots) are evident in the circled areas. Carbon clustering scavenges the conductive constituents from large areas of the adhesive, which are thus able to charge up to significant potentials that facilitate dielectric discharge.

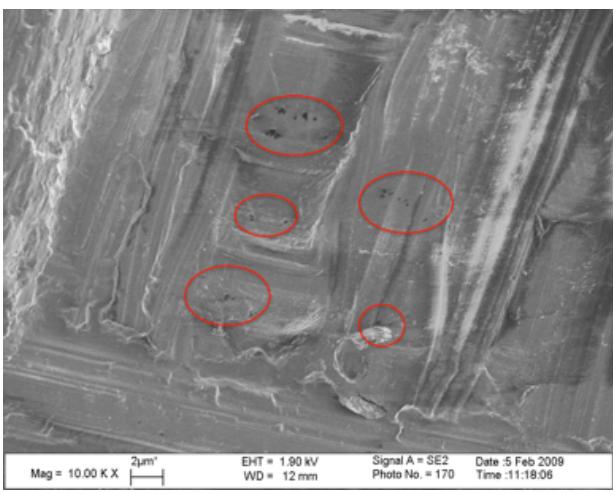

Figure 4. SEM imaging of 5% carbon loaded adhesive.

As a final check, a complete patch assembly comprising a graphite-composite with aluminum skins patch element, carbon-loaded Astroquartz honeycomb, support panel and 50Ω impedance RF feed was subjected to a 600 keV, electron flux of up to 25 pA/cm^2. The RF feed of the patch antenna was monitored for discharge pulses using an oscilloscope. This test was performed at the Van de Graff Facility at Goddard Space Flight Center. Tests were performed at room temperature and -60°C. The test article is illustrated in Figure 5 configured for normal incidence of electron flux. Testing with side incidence was also performed. The resulting pulses of the order of 6 V for normal incidence (Figure 6) and 9 V for side incidence were considered an unacceptable disturbance for the Juno instruments.

Figure 5. Patch with 0.38% BP2000 carbon-loaded Astrquartz honeycomb in target area assembly prepared for normal incidence test.

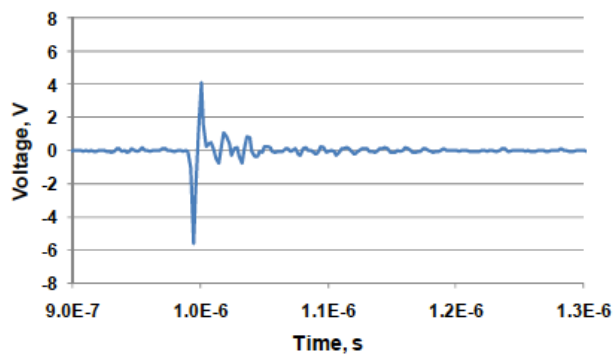

Figure 6. Discharge transient of carbon-loaded patch test article depicted in Figure 5. The main pulse is about 10ns duration and dies to zero in 5 rings.

4.2 Feed Network

The power divider/combiner assemblies were the most complicated components of the patch arrays antennas, in terms of construction. Figure 7 shows a schematic of the power divider/combiner assembly. The circuit that produces the power splitting (and tapering) from the antenna elements is implemented by means of an air-stripline circuit. The copper circuit traces are printed on a thin circuit board suspended between two halves of the machined aluminum housing. The traces have an electroless nickel emersion gold (ENIG) finish. The top and bottom parts of the housing are joined together using fasteners, making the part reworkable. The thin circuit board is supported by a shelf along the periphery and at various points in the interior by ridges machined into the housing. Additionally, the housing is slightly oversized and the board is able to 'float' to accommodate shrinkage in the housing as the unit is cooled.

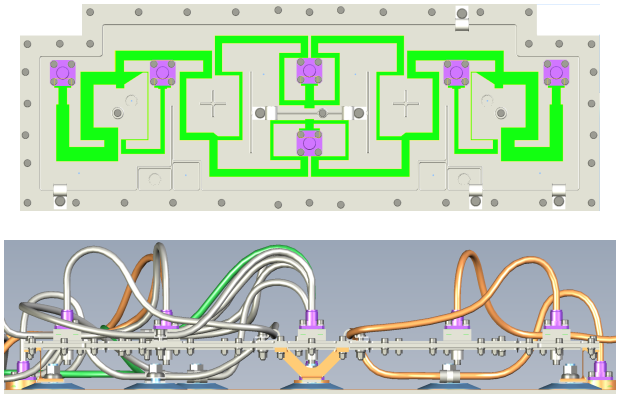

Figure 7. Top: A2 power divider/ combiner top-view showing stripline circuit (green) and coaxial interconnects (purple). Bottom: side-view showing mounting flexures and coaxial cable attachments.

The interconnect between the circuit board to coaxial connector is illustrated in Figure 8. The connector probe extends into a cylindrical sleeve machined into the aluminum housing, and a ribbon is soldered to the end of the probe, passes through a slot in the sleeve, and is soldered to the trace on the circuit board. The process of solder attachment was qualified earlier in the development. We tested both tinned copper ribbon of thickness 2 mil and width 40 mil, as well as beryllium copper ribbon of the same dimensions. A series of coupons were fabricated that allowed the circuit board to displace up to ±20 mil relative to the pin, simulating a mechanical stress on the ribbon consistent with allowable board movement in the divider/combiner assembly. The two sets of ribbons were subjected to a round of mechanical stress, followed by thermal cycling (-185°C to +120°C), followed by a second round of mechanical stress, and were then pull tested to failure. The required MIL-STD 883 minimum break force was 110 g. The stressed tinned copper samples had a break force of at least 8 times the requirement. The stressed beryllium copper ribbons were twice as strong. However, the beryllium copper ribbons were less compliant than the tinned copper ribbons, which made them harder to form and possibly more susceptible to tearing. We also considered attachment processes like ribbon welding, but soldering offered better flexibility and reworkability.

Prior to final solder assembly, the interconnect ribbon was tinned with solder (to prevent tin whiskers) and one end was soldered to the coaxial probe. The connector was attached loosely to the boss on the housing and the ribbon was shaped and soldered to the circuit board. The connector was then adjusted slightly using a microscope to position it centrally in the cylindrical sleeve. Proper alignment of the probe and proper shaping of the ribbon was a meticulous process that took a fair amount of time to develop. The thread insert for a screw that is used to securely fasten the top and bottom halves of the housing can be seen in Figure 8.

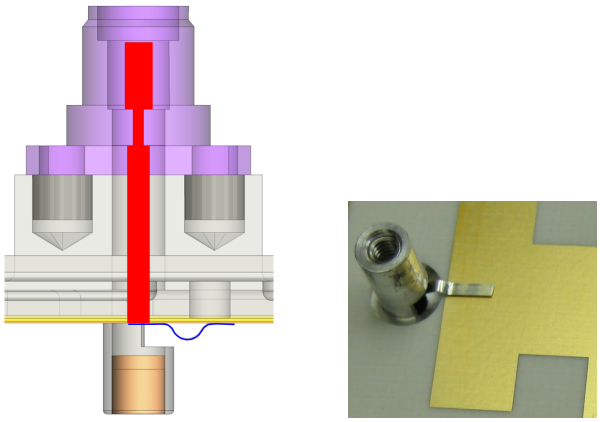

Figure 8. Power divider/combiner interconnect. Left: coaxial probe (red) and ribbon (blue) attached to circuit board (yellow). Right: photo of bottom view of circuit board prior to solder assembly.

The power divider/combiner circuits were realized as unequal-power Wilkinson circuits with quarter wave impedance transformers. Wilkinson dividers require a resistor to provide isolation. We selected thin film chip resistors in a 0705 surface mount package for these isolation resistors. The resistance values are approximately 100 ohms with 0.1% tolerance. The temperature coefficient of these resistors is ±25 ppm/°C. As the Juno temperature range exceeds the normal Mil-Spec range, the resistors were qualified by thermally cycling them between -185°C and +120°C while monitoring their resistance. The resistors were soldered to the circuit board.

The substrate for the power divider stripline circuits is dielectric and is susceptible to bulk electron charging by Jupiter high-energy electron fluxes, even though it is partially shielded by the aluminum power divider housing. Because the dielectric material is quite thin (0.3 mm) we could provide adequate self-discharge capability by coating the back side of the printed circuit board with a high resistivity germanium film. The germanium film in the MWR application had a surface resistivity of 2.8×10^{8} ohm per square and needed to be less that 10^{12} ohm per square specifically for this circuit board application to provide adequate discharge. The film side of the printed circuit board was grounded to the power divider/combiner housing at multiple locations using small springs.

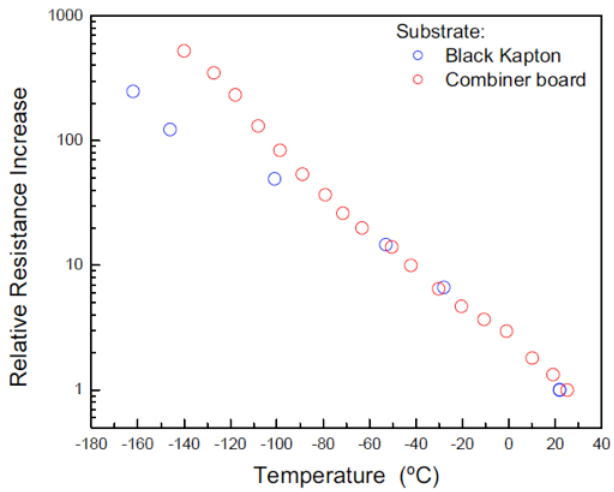

Figure 9. Germanium thin film relative resistance versus temperature. Nominal resistivity at room temperature is 10^8 ohm per square.

Germanium is well suited for our application because in thin layers it provides very little RF loss. However germanium is a semiconductor with the result that its conductivity is a strong function of temperature. Figure 9 illustrates that the resistivity of a 1215 Angstrom thick germanium film can increase by almost 3 orders of magnitude over the Juno MWR antenna temperature range. Even though the surface resistivity is at the limit of the acceptable range at worst-case cold temperatures, this thickness of germanium provides an adequate electron bleed for the partially shielded stripline dielectric. The power divider/combiner circuits were not subjected to electron charging tests in the manner of the patch elements and coaxial cables. Instead, IESD performance was assessed by analysis. It was calculated that the largest potential difference that would be generated across the printed circuit board in the Jupiter environment is 10V, which was sufficiently low as to not be a concern.

The RF losses associated with adding the germanium coating were also assessed. During the fabrication and assembly of the engineering model (EM) antennas, spare power divider/combiner assemblies were produced for both the A1 and A2 antennas. The RF losses of these spare units, as well as the units that were installed on the antennas, were measured as part of the sub-assembly test acceptance procedure. During the course of EM fabrication, germanium coatings were not applied to the power divider/combiner hardware. The printed circuit board was removed from the spare A2 EM power divider/combiner and was coated with germanium. The board was then reassembled into the spare A2 unit and the insertion loss was re-measured using a vector network analyzer. The coating was found to add 0.05dB of insertion loss at room temperature. As there are a total of two power/divider circuits in series with any given antenna element and the output port of the entire antenna, the total loss is 0.1dB. This was deemed to be acceptable. Furthermore, the loss at cold operating temperature would be expected to decrease, and the loss for the lower frequency A1 antenna would also be expected to decrease.

The coaxial cables that are used in the MWR A1 and A2 antennas were tested at the Goddard Van de Graff facility. Two coaxial cables (0.142" diameter and 0.2" diameter) are shown mounted on a carbon-loaded black Kapton film in the target area assembly in Figure 10. The MWR A1 and A2 feed network cables are 0.142" diameter, and the cable connecting each antenna to its respective radiometer receiver is 0.2" diameter. The cables were exposed to an electron flux of 4-25 pA/cm^2 at 1.4 MeV and showed no evidence of internal electrostatic discharge. This is attributed to the shielding provided by the jacketing of the cables.

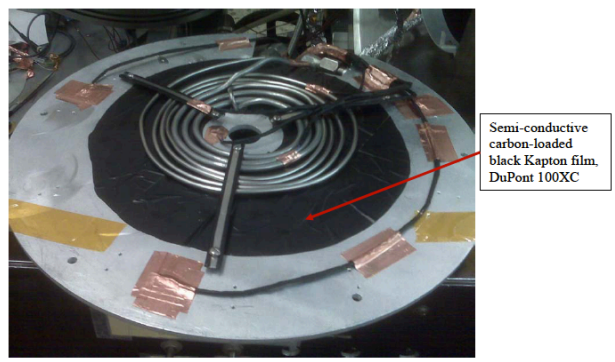

Figure 10. Coaxial cables mounted on black Kapton in target area assembly.

Originally, the plan was to perform protoflight environmental testing of the fully assembled EM antennas. However, partial delamination of patches from the carbon-loaded Astroquartz substrates precluded this, so instead this testing was performed on power divider/combiner sub-assemblies. The testing included thermal atmosphere cycling, vibration testing, and pyroshock testing.

Extensive thermal atmosphere testing of the spare A1 EM power divider/combiner assembly, as well as an early prototype version, was performed over temperatures exceeding the protoflight temperature range, to assess RF performance. It was during testing of the prototype unit that we discovered anomalous behavior in the return loss performance over temperature. This was later traced to gapping in the two halves of the power divider/combiner housing at the location of the coaxial interconnects. We later devised a method to attach the housing halves firmly together at each of the 6 coaxial interconnects. This detail was critical to obtaining stable performance over temperature.

Figure 11 illustrates the A1 power divider/combiner during random vibration testing at JPL. The divider/combiner assembly is mounted on four V-shaped flexure brackets that attach to surface mount studs, or in the case of the test to the vibe fixture. Flexures are used to mount the power dividers/combiners to accommodate differential thermal expansion between the aluminum power dividers and the graphite-composite facesheets of the support panel. Spare

coaxial cables were also attached to the assembly, as these are an integral part of the structural design, providing stiffness and damping. The protoflight limits were nominally 20.3 grms in the X-axis and Y-axis, and 40.6 grms in the Z-axis (normal to the plane of the power divider/combiner assembly). The tests were performed for 1 minute on each axis. The overall measured input acceleration in the Z-axis was 38 grms due to notching caused by force limiting. The Z-axis vibration response was highest at 71.1 grms on the A1 power divider/combiner at a point roughly half way between the middle and end flexures. Following vibration and shock testing, RF S-parameters of the test article were re-measured to ensure RF performance had not changed.

The fact that the power dividers/combiners performed successfully after these very high vibration levels without any modifications was a major achievement in the antenna design.

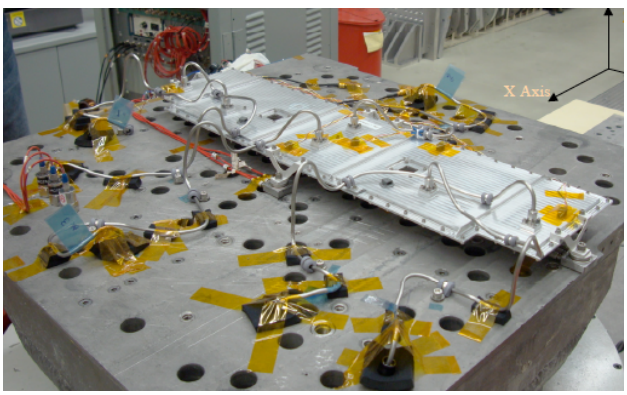

Figure 11. A1 EM power divider/combiner mounted for Z-axis vibe test.

4.3 Support Panel

In order to minimize the mass of the antennas, the support panels were made up of graphite-cyanate ester composite face sheets only 0.25 mm thick and of the lightest aluminum honeycomb core density practicable. The main core for the A2 antenna was 1.0 pcf density but the bigger A1 antenna had 1.6 pcf density due to the higher acoustic loading that it experienced. For both antennas a higher density 3.1 pcf core was locally spliced in at the 4 attachment points for each antenna. At each attachment location a graphite composite doubler was bonded to the thinner facesheets. For the A1 antenna, 2 of the attachments interior to the panel had a pattern of 4 threaded insets bonded to the core. The remaining 2 attachments at the edge of the A1 panel had an aluminum block with a 4 bolt pattern bonded to the aluminum honeycomb core and bolted to the 2 doubler plates bonded to the face sheets on both sides of the panel. For the A2 antenna all of the attachment points were interior to the panel and were identical to those interior to the A1 panel.

As part of the qualification of the antenna panels a small structural test panel, illustrated in Figure 12, was constructed from flight-like materials and with representative attachment points in order to establish the load capability of the attachments. The test panel was first thermally cycled, proof loaded and then load tested to failure for each type of attachment fitting. The first test panel was compromised due to a shortcoming of the initial test fixture and a second had to be constructed. The cost of the structural panel test program was very worthwhile because the load testing did indicate that, for the top fittings, the core was being overloaded along the top of the panel at maxim loading. This design deficiency was corrected for the already manufactured flight A1 panel by adding an extra shear strip along the top of the panel.

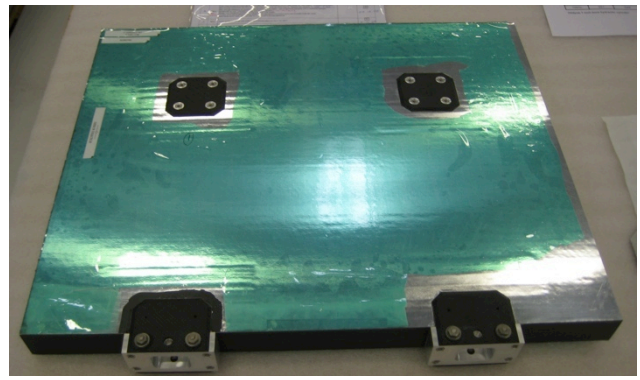

Figure 12. Antenna support panel structural test article.

The flight panels then underwent proof loading uneventfully before and after thermal cycling. Figure 13 shows one of the tests on the A2 flight panel.

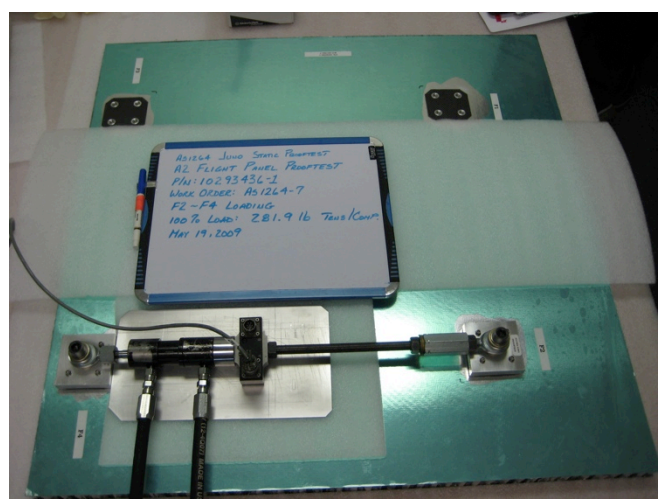

Figure 13. A2 antenna support panel proof load test.

As a matter of course all the surface mount fittings bonded onto the support panels were also proof loaded. An example test is shown in Figure 14.

Figure 14. Surface mount fitting proof load testing.

4.4 Summary

In summary, this Section has discussed in detail the process by which we developed materials and processes for the MWR antennas. Significant effort was put into selecting, and in some cases engineering, materials to perform in the Jupiter environment

The use of carbon loading of the Astroquartz honeycomb and attachment adhesive to provide self-discharge proved to be unsuitable for the MWR antenna application. Shortly after the fabrication of the A1 EM antenna, we noticed partial delamination of patches from the carbon-loaded Astroquartz honeycomb substrate. While subsequent process refinements helped improve adhesion, there appeared to be no way to simultaneously achieve good mechanical adhesion, low RF loss and freedom from electron charging and arcing. The carbon loading process turns out to be very difficult to optimize because the conductivity relies on the tendency of the carbon particles to aggregate into a network of connecting tracks. Below a certain carbon loading level the carbon tracks become isolated chains, no longer forming a connecting network, and the volume conductivity drops precipitously. The preferred RF properties occur near this conduction threshold, which proves to be very hard to predict because it depends critically on the dispersion of the carbon and is highly process dependent.

We took an unconventional approach to developing the feed networks for the antennas, choosing a mechanically-oriented design for the divider/combiner comprising machined housings, suspended circuit boards, and hundreds of fasteners. This approach influenced the design of metal patch antenna element that would eventually replace the carbon-loaded Astroquartz patch. The development of this new antenna element is described in the following Section.

5. METAL PATCH DEVELOPMENT

During the time that the MWR antenna team was experiencing difficulties in meeting performance requirements with the carbon-loaded patch design described in the previous Section, an alternative antenna element concept was explored by the team. The genesis for this concept came from a study that was performed earlier on in the development to assess the impact of micrometeoroids on RF performance.

A worst case damage assessment was performed by assuming that a micrometeoroid would form a short circuit between the patch and ground, depositing an electrically conductive trail on the Astroquartz honeycomb substrate. The analysis, which involved computing the return loss and the pattern of the patch, was performed exhaustively for a matrix of short circuit positions covering the patch. When the results were analyzed, it became apparent that the patch was able to perform reasonably well with the short circuit distributed over a fairly large area toward its center. It is well known that a half wave resonant patch effectively has a short circuit at its center (the initial MWR patches had a grounding wire at this location). However, what was not known at the time, until this micrometeoroid study was performed, was that the grounding 'wire' could be quite large; indeed it can be large enough to support the patch itself without the need for a dielectric substrate. This hypothesis was later verified by performing RF analyses in HFSS, and the metal patch concept was born.

The initial metal patch concept was presented to MWR management on January of 2009. The initial concept featured a rectangular metal patch mounted on a circular, centrally located support column, machined from a block of high grade aluminum. Based on the successful testing and performance of the A1 and A2 power/divider circuits, materials and machining processes that were utilized for the housings of these assemblies were proposed for the metal patch. The patch would attach to the existing panel hardware using the same surface-mount stud that is used for attaching power divider/combiner and coaxial cable hardware to the rear of the panel. The probe interconnect would be via a slip-fit receptacle integrated into the patch body. The concept is depicted in Figure 15.

The concept, it later transpired, would be remarkable from a number of different perspectives. First, by design, it eliminated the issue of IESD by eliminating dielectric from the construction. Second, it required very little modification of the existing panel and feed network hardware. The interconnect probe tips had to be modified by attaching a bullet that would mate with the receptacle in the patch, and the support panel had to be fitted with surface-mount studs to attach the patches. Third, the attachment process is much easier for metal patches than the previous design, and could be done as a final step in the antenna assembly allowing later delivery (in the previous design, patches are the first items to be attached to the support panel). The metal patches attach to the stud with a nut that provides a preload against forces that would be experienced during launch. The slip fit probe is much easier to assemble than the soldered probe of the previous design. Fourth, metal patches are reworkable and replaceable, and this capability was utilized throughout the development and beyond. Fifth (and this was not realized at the time of conception), metal patches have

superior thermal properties and do not require special coatings to mitigate the effects of heat loading during launch. Sixth, initial mass estimates showed modest growth relative to the previous design.

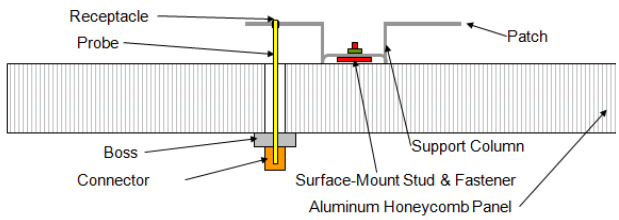

Figure 15. Initial metal patch concept showing mounting and interconnect approach. The patch geometry was later modified to provide greater stiffness.

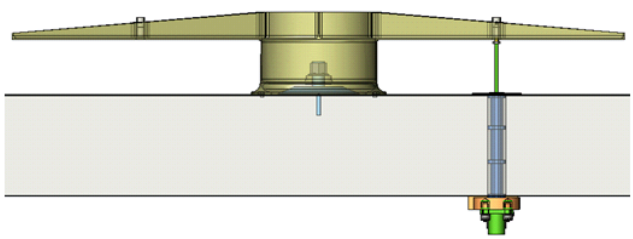

Figure 16. Metal patch featuring stiffening ribs and tapered pedestal foot.

MWR management approved the initial metal patch concept for further study and development. It should be noted that this development was done in parallel with the flight build of the antenna support panels and feed network hardware. In order to limit the deflection of the cantilevered patch edges, particularly at the probe connector locations, we added stiffening ribs to the top surface of the patch, as depicted in Figure 16. The resulting design for the metal patch element had a first mode greater than 200 Hz.

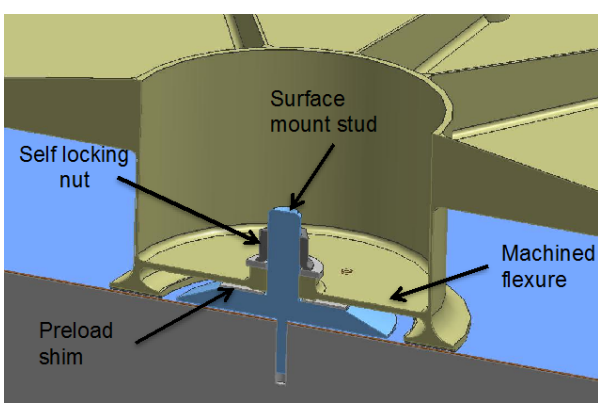

Figure 17. Illustration of flexure and preload to Click Bond stud.

Perhaps the most challenging aspect of the structural design of the metal patch was in the design of the panel attachment features. As illustrated in Figure 17, the patch is supported on a cylindrical pedestal and the attachment to the panel must provide the following features: 1) precise location; 2) accommodate differential thermal expansion between the aluminum pedestal and the graphite composite panel; 3) withstand launch loads; and 4) maintain electrical contact around the base of the pedestal. This was achieved by attaching the pedestal to a surface mounted stud through a flexure disk machined into the patch element (illustrated in Figure 17). A shim stack is set for each patch element to deflect the disk a precise amount to apply a controlled preload around the base of the pedestal. Preload provides the necessary electrical contact and allows some slipping during thermal cycling. The amount of preload is a balance between providing sufficient overturning moment for launch loads and not crushing the light-weight honeycomb support panel.

For the A1 metal patch, this required a flexure thickness of 0.81 mm that would deflect by 0.25 mm when the nut on the stud is torqued down. The 0.25 mm deflection was controlled by placing precision shims over the surface mount stud and the resulting preload of 592 N over the 7.6 mm wide pedestal foot would prevent gapping under load. For the A2 metal patch, the flexure thickness was 0.18 mm. The precision and associated tolerances for machining these parts were extremely demanding. It is also remarkable that the support panel, originally designed for Astroquartz patch, did not require any modification for attachment of metal patches.

As the structural analysis proceeded, it became necessary to strengthen and modify different parts of the patch geometry, but overall the patch thickness did not change from the 0.5 mm thickness of the initial concept (the same thickness as the power divider/combiner housings). The patch also features two interconnect receptacles but only one probe connection. The second receptacle was added to provide greater symmetry, thus reducing tipping moments under vibration. Additionally, at the time we had not fully qualified the receptacle approach, so having a spare receptacle was seen as a possible contingency.

For the stud attachment we used a high performance structural adhesive. This adhesive has excellent tensile lap shear strength (>4000 psi) at room temperature and approximately half of the room temperature strength at the maximum flight allowable temperature range. The bond line was controlled to 0.25 mm thickness by placing glass beads in the adhesive prior to application. The fact that the adhesive and the beads are dielectrics is not an issue, as these materials are captured within a Faraday cage formed by the flexure of the metal patch, the foot of the circular patch support pedestal, and the panel. This cavity was vented by placing two small channels in the pedestal foot. For the A2 metal patch, we used the same Click Bond™ surface mount stud that was used for the A1 metal patch, only with the carbon graphite foot of the stud trimmed to fit within the smaller inside diameter of the A2 pedestal.

Other refinements to the design were made as the metal patch development unfolded. The probe receptacle was implemented using a unique hyperboloid contact design (Hypertronics Hypertac) that facilitated hundreds of thousands of insertions and extractions, with no noticeable degradation in performance. This receptacle has very desirable performance with respect to vibration at launch, and good contact over the Juno temperature range. The receptacles are soldered into a copper plated socket machined into the center most rib of the patch (Figure 18).

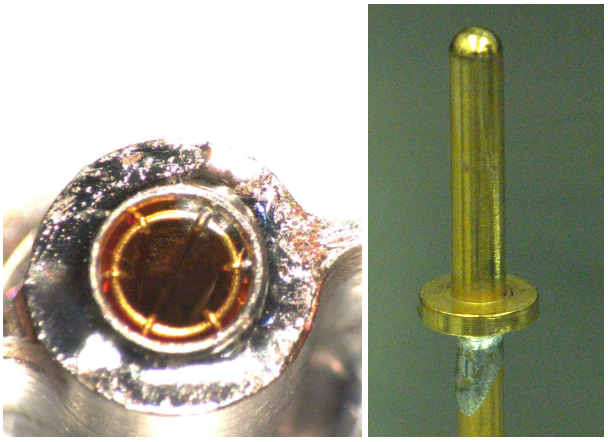

Figure 18. Left: Hyperboloid multi insertion receptacle. Right: Probe tip with soldered mating bullet. (Photos at different scales.)

Eliminating composites from the design of the patch element greatly simplified both the mechanical and RF analyses of the patch. The simple, monolithic construction of the patch and its simple attachment method made it amenable to very precise finite element analysis (both for structural design and RF design purposes). This was the complete opposite situation of the previous design, and was instrumental in allowing us to achieve first pass success with the two metal patch designs.

Following the promising results from the design phase, an engineering qualification model (EQM) of the A1 metal patch was fabricated and subjected to a series of tests to assess its performance and qualify it for flight use. The first tests we did were RF measurements to determine the accuracy of the tuning. Vector network analyzer measurements of the return loss of the measurement showed a resonant frequency that was within 0.05% of the HFSS predictions. This level of precision was unprecedented in our previous measurements of dielectric patches and is attributed to the elimination of dielectrics, which always presents an uncertainty in tuning a patch element. Next, the patch was thermally cycled (in atmosphere) over the protoflight temperature range of -135°C to +120°C. RF measurements made after the thermal cycling did not change from those made before. Additionally, the patch maintained is shape and dimensional tolerances, and remained firmly attached to the test support panel. However, to more thoroughly assess the structural performance of the stud, a separate set of pull tests were made on stud coupons that were both thermally cycled and not. Following thermal cycling, the EQM A1 patch was subjected to a vibe test at the full protoflight level of 40 grms.

The EQM A1 metal patch passed all of these tests on the first attempt which allowed us to implement the design in the flight antenna hardware. No prototyping of the A2 metal patch was done; we went straight to production of the flight articles from design (Figure 19). The A2 antenna performed precisely according to predictions.

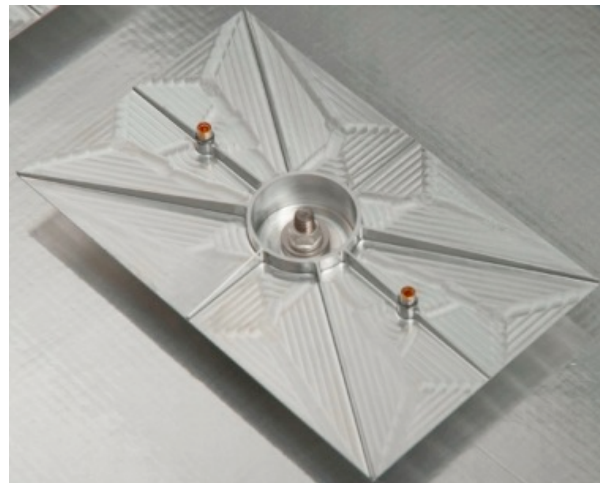

Figure 19. A2 metal patch element

The mass of the protoflight A1 and A2 antennas is 13.84 kg and 4.88 kg respectively. The combined mass is 0.1 kg less than the combined mass of the antennas as estimated at CDR following the EM build (including anticipated mass growth to increase strength of the FM support panel). It is interesting to compare the original and final mass allocations of MWR antenna masses (Table 4).

Table 4. Antenna mass.

Antenna	Initial Mass (CSR)	Final Mass (HRCRs)	Mass Growth
	(kg)	(kg)	(%)
A1	10.0	13.84	+38.0
A2	5.0	4.88	-2.4
A3	3.9	7.25	+85.9
A4	1.0	1.46	+46.0
A5	0.3	0.51	+70.0
A6	0.5	0.75	+50.0
Frame	-	4.82	-
Total	20.7	33.51	61.9

At the time the MWR instrument was proposed, the A1-A5 antennas were conceived as slot arrays and the antennas were all conceived as attaching directly to the spacecraft. Later, for testing and performance purposes, the A3 and A4 antennas were mounted together on a frame that added 4.82 kg to the total mass. Relative to the original allocation, the

patch array antennas resulted in the lowest fractional mass growth, with the A2 antenna being the only antenna to show a decrease in mass. Not including the frame, the largest slot array (A3) had the largest fractional mass growth of 86%. These results vindicate the decision to change the A1 and A2 designs from slots arrays to patch arrays.

6. ANTENNA SUBSYSTEM TEST AND VERIFICATION

As described in the previous sections, the final protoflight versions of the MWR patch array antennas were more or less the same as the versions originally conceived at the beginning of the EM phase, with the exception of the new metal patch element. Considerable effort was put into developing and qualifying components for these antennas, and into refining the EM design to improve performance margins. The MWR A1 and A2 antennas are essentially brand new designs that attain state-of-the-art performance in a very demanding environment. The final protoflight qualification was performed on the top-assembly antennas. This testing included thermal vacuum testing followed by acoustic testing, and is described as follows.

Following completion of fabrication and assembly of the A1 and A2 protoflight antennas, antenna patterns were measured in a spherical near-field antenna range facility at Nearfield Systems Inc (NSI). This facility has the capability to accurately measure a full sphere at the relatively low operating frequency of the A1 antenna. The five other MWR antennas were also measured at the NSI facility. These measurements provided a performance baseline. The original plan was to make a second set of antenna pattern measurements after environmental testing to assess any perturbations caused by the testing. However, for cost reasons, the second set of pattern measurements was descoped, with the exception of the second set of A2 measurements. Figure 20 shows the A1 antenna being mounted for testing in the NSI facility.

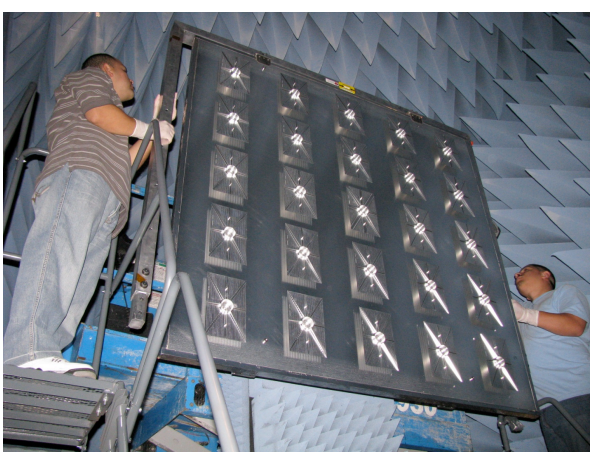

Figure 20. A1 antenna being mounted for pattern measurement at NSI.

Results from the A1 and A2 RF measurement campaigns are discussed in detail in [6,8]. These results showered very good agreement with predictions from simulations. During the testing of the A2 antenna, a loose cable resulted in an anomalous pattern measurement. The loose cable was not detected by an earlier return loss measurement at JPL prior to the pattern measurement. Therefore, a new method of assessing antenna integrity, termed *Impulse Testing*, was devised to check the antennas before and after various environmental tests [9].

Thermal Vacuum testing

The A1 and A2 antennas were tested together in thermal vacuum for which the test objectives were as follows:

1. Obtain thermal balance measurements for both worst-case hot and worst-case cold environments
2. Verify the thermal math model of the antennas
3. Cycle the antennas (two times) between upper and lower protoflight temperatures, holding at each temperature extreme for 12 hours
4. Bakeout antennas at 100°C in near vacuum for at least 48 hours
5. Characterize thermal time constant of antennas

The Environmental Requirements Document (ERD) called for three thermal cycles in vacuum, but this was descoped to two cycles in view of the fact that the flight support panels had been cycled three times (in atmosphere) over the protoflight temperature range, and that the A1 metal patch EQM and elements of the feed network had been thermally cycled numerous times (also in atmosphere).

A summary of the thermal vacuum test matrix is presented in Table 5. The test duration was nominally 270 hours. The vacuum pressure was controlled at less that 10^{-5} torr, with the exception of the cold qualification cycles, the initial pump down and the return to ambient, where the requirement was relaxed to $2x10^{-5}$ torr. The temperatures in Table 5 are the chamber set points; not the temperatures of the antenna.

Table 5. Summary of thermal vacuum test conditions.

Phase	Chamber	Duration
	(deg C)	(hrs)
Pump Down	20-105	12
Bakeout (1st half)	105	24
Hot-Qual 1st cycle + ¼ bakeout	123	18
Hot Balance	105	19
Cold Balance	-185	44
Cold Qual 1st cycle	-180-155	52
Hot Qual 2nd cycle + ¼ bakeout	123	32
Cold Qual	-180-155	52
Return to ambient	-180-45	17

The test was performed using JPL's 7-foot cylindrical chamber. This chamber has three shrouds; one around the circumference and one at each end of the cylinder. A flat secondary shroud was added in front of the antenna

radiating faces for tighter thermal control. The shrouds are operated with liquid and gaseous nitrogen and could be controlled to a wide temperature range. During the thermal balance portion of the test, the chamber simulated the spacecraft, providing a radiative boundary condition for the back of the two antennas. The antennas were mounted on a custom fixture and were dressed with flight-like MLI blankets (Figure 18).

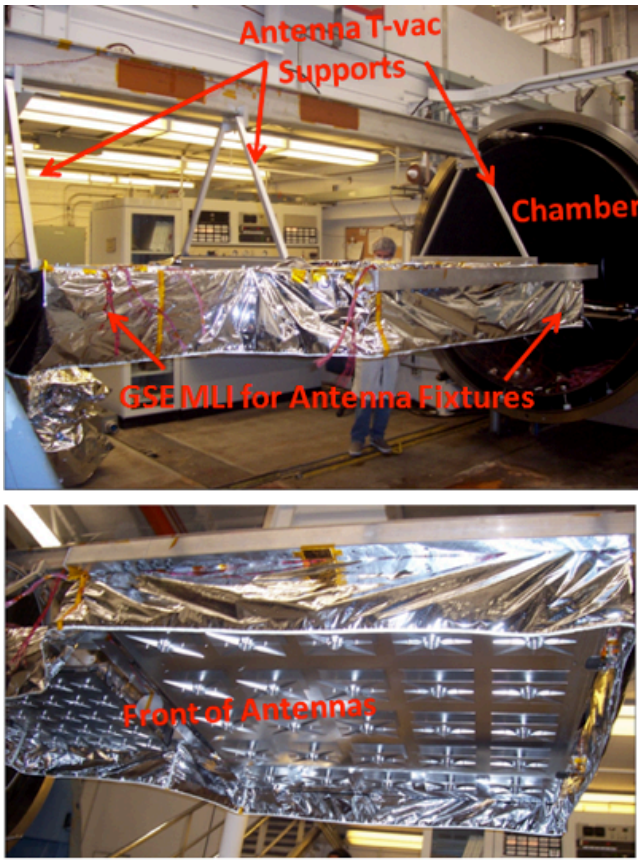

Figure 18. A1 and A2 antennas being prepared for thermal vacuum testing.

A conductive boundary condition temperature was maintained with film heaters at the eight handling fixture interface brackets. The temperature controlled interface brackets simulated the spacecraft's mechanical attachments to the antennas. Temperature measurements were taken with 15 thermocouples on the A1 antenna, 14 thermocouples on the A2 antenna, and an additional 12 thermocouples on the handling fixtures.

Following successful completion of the thermal vacuum test, the thermal model parameters were adjusted to provide better correlation of predictions with results. Pre-test predictions varied from measurements by ±10°C, post-test predictions varied by ±3°C.

Impulse Test measurements were made on the A1 and A2 antennas before and after thermal vacuum testing and showed no evidence of change.

Acoustic Testing

The A1 and A2 antennas are shown mounted on their acoustic/handling fixtures in Figure 19. For the A1 antenna, we employed the turnover fixture that was used for antenna assembly as the acoustic test fixture. Acoustic testing was performed at JPL's Environmental Test Lab. The A1 and A2 antennas were instrumented with 5 triaxial accelerometers each, and 10 force transducers at the 4 mounting points to measure interface forces. Acoustic test control instrumentation consisted of 8 control microphones and 4 monitor microphones hung from the test chamber ceiling. The overall SPL was measured as 140.3 dB. The protoflight (PF) acoustic specification was met at all frequencies from 31.5 to 1000 Hz and at or near the tolerance for frequencies of 1250 Hz and above.

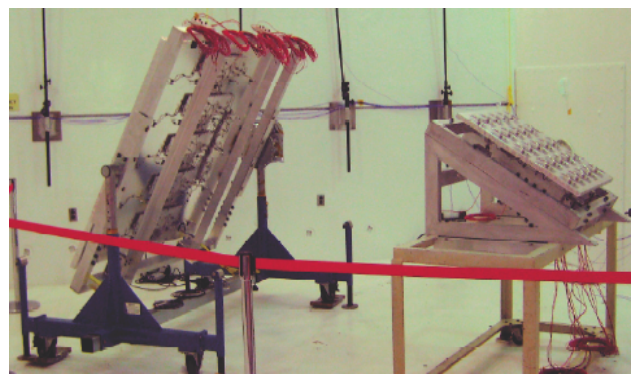

Figure 19. Acoustic test setup. A1 antenna (left). A2 antenna (right).

The response at the A1 antenna center was 8.5 grms, and 20.2 grms at the center of one of the power divider/combiner assemblies. The highest Z-axis antenna mount force was measured as 97.4 Nrms. The response at the A2 antenna center was 11.0 grms, and 4.5 grms at the center of one of the power dividers. The highest Z-axis antenna mount force was measured as 36.5 Nrms. Pre and post test PF-9 dB low level test run overlay plots revealed no significant mode shifts in either antenna. Impulse Test measurements were made on the A1 and A2 antennas before and after acoustic testing and showed no evidence of change. Additionally, pattern measurements were made on the A2 antenna and these showed very good agreement with the measurements that were made before environmental testing.

7. SUMMARY

This paper has discussed the development of patch array antennas for the Juno Microwave Radiometer Instrument. The antennas were designed to meet very demanding performance requirements. In particular, considerable effort was put into developing and qualifying materials to mitigate the effects of electron charging and subsequent internal electrostatic discharge (IESD) near Jupiter.

The initial approach that we adopted for eliminating IESD in the patch dielectric substrate turned out to be impracticable. Consequently, we developed a new type of patch antenna element that eliminates dielectric from the design, thereby eliminating the issue of IESD in the antenna element. This design philosophy of either eliminating or minimizing dielectric is also evident in the design of the feed networks. The power divider/combiners were constructed as thin stripline circuits with aluminum housings integral to the circuit function. The final antenna designs prominently feature machined aluminum parts and thousands of fasteners, which is a radical departure from patch array antennas that conventionally employ printed circuit board-based composite construction.

Qualification testing of components and sub-assemblies, as well as protoflight testing of the full antenna assemblies, was described. Antenna pattern measurements and another electrical testing technique developed specifically for the program showed no impact to RF performance from environmental testing.

Despite heavy reliance on metal parts, the A1 and A2 antennas showed negative growth relative to mass estimates at Critical Design Review, and these antennas had the lowest mass growth of all MWR antennas relative to estimates at the beginning of the mission.

The A1 and A2 antennas were delivered to the instrument team for integration and test (I&T) in December 2009, two years after the antenna sub-system Preliminary Design Review in December 2007 and 14 months after the Critical Design Review in October 2009. It is estimated that the issues associated with developing the carbon-loaded patch element resulted in a 10 week delay in delivering the antennas to instrument I&T. The metal patch development is estimated to have taken 14 weeks. The mission successfully launched on August 5th 2011. Three weeks later, during preliminary check out of the MWR instrument, it was confirmed that all 6 of the radiometer receivers were properly receiving microwave signals from the galactic plane through their respective antennas.

8. References

[1] "Internal Electrostatic Discharge Environment at Jupiter", H. B. Garrett, R. W. Evans, Spacecraft Charging Technology Conference, Noordwijk, The Netherlands, 2001.

[2] "Microwave Radiometers from 0.6 to 22 GHz for Juno, A Polar Orbiter around Jupiter", P. Pingree et al, IEEE Aerospace Conference, Big Sky, MT, 2008.

[3] "A look Inside the Juno Mission to Jupiter", R. Grammier, IEEE Aerospace Conference, Big Sky, MT, 2009.

[4] "Key and Driving Requirements for Juno Payload Suite of Instruments", R. Dodge, M. A. Boyles, C. E. Rashbach, AIAA Space Conference & Exposition, CA, 2007.

[5] "Juno Microwave Radiometer Patch Array Antennas", N. F. Chamberlain et al, IEEE APS/URSI Conference, Charleston, SC, 2009.

[6] "Juno Microwave Radiometer All-Metal Patch Array Antennas", N. F. Chamberlain et al, IEEE APS/URSI Conference, Toronto, Canada, 2010.

[7] "Guide to Mitigating Spacecraft Charging Effects", H. B. Garrett and A. C. Whittlesey, JPL Space Science and Technology Series, Joseph H. Yuen, Editor-in-Chief, Jet Propulsion Laboratory, California Institute of Technology.

[8] "Accurate loss measurements of the Juno patch array antennas", N. F. Chamberlain, et al, IEEE Phased Array Conference, Boston, MA, 2010.

[9] "Impulse Testing of Corporate-Fed Patch Antenna Arrays", N. F. Chamberlain, IEEE Aerospace Conference, Big Sky MT, 2011.

[10] "Low-Sidelobe Slot Arrays for the Juno Microwave Radiometer", M. Zawadzki et al, IEEE APS/URSI Conference, Toronto, Canada, 2010.

[11] "Contamination and ESD Control in High Technology Manufacturing", R. W. Welker, R. Nagarajan, C. E. Newberg, Wiley-IEEE Press, 2006.

[12] "Carbon Black: Science and Technology," edited by J.B. Donnet et al, Dekker, New York, 1993.

[13] "Microwave Characterization of Filled Polymers", C. Brosseau et al, J. Appl. Phys. **89 (8)**, 4532, 2001.

[14] "Non-conductive specimens in the electron probe microanalyzer—a hitherto poorly discussed problem", G. F. Bastin and H. J. M. Heijligers, in Electron Probe Quantification, p. 193, edited by K. F. J. Heinrich and D. E. Newbury, Plenum, New York, 1991.

[15] "Control of charging in low-voltage SEM", D. C. Joy, Scanning **11,** 1, 1989.

9. BIOGRAPHIES

Richard Hughes *received a B.Sc. in Honours physics from the University of Manitoba, Canada in 1970 followed by a Ph.D. in Solid State Physics in 1975 from Simon Fraser University, Canada. He worked at the Canadian Defence Research Establishment Atlantic in Nova Scotia from 1974 through 1984 and then spent 5 years at the Canadian National Research Council in Ottawa. From 1989 through 2006 he held various engineering, R&D and management positions at Astro Aerospace in Carpenteria, California including being the Chief Engineer for the ISS Mobile Transporter. For the last 5 years he has been a Mechanical Systems engineer at JPL in the Instrument Mechanical Engineering Section specializing in flight antenna systems including leading the mechanical engineering effort for the Juno Microwave Radiometer antennas.*

Neil Chamberlain *received the B.Sc. with Honours from Kings College London, UK in 1981. He worked briefly for Marconi Space and Defence Systems, Ltd., Portsmouth, UK before undertaking graduate studies at The Ohio State University, where he received the M.S. and Ph.D. degrees in Electrical Engineering in 1984 and 1989, respectively. He was a professor at the South Dakota School of Mines and Technology in Rapid City, South Dakota between 1990 and 2003. His research focused on ultra-wideband radar antennas and systems. He is currently a Senior Engineer with JPL's Flight Spacecraft Antennas Group, where he was recently involved in developing antenna arrays for UAVSAR and Juno Microwave Radiometer Instrument. He is currently leading the antenna development for the DESDynI synthetic aperture radar instrument.*

Julie Jakoboski *received a B.S. in Mechanical Engineering and a B.A. in Physics from Bucknell University, USA in 2007. As a student, she worked in the Optics Group at Paranal Observatory, ESO, Chile on the VLT Interferometer. After graduation, she joined JPL as a Mechanical Engineer in the Opto-mechanical Engineering Group. Currently, she works in the Antenna/Reflector Design Group at JPL.*

Mihail P. Petkov *received a B.S. degree 1987, and M.S. in Physics in 1989 from the University of Sofia, Bulgaria. He obtained his Ph.D. in Physics from Washington State University in 1998. Mihail is a Senior Failure Analysis Engineer at the Jet Propulsion Laboratory, California Institute of Technology. His research interests include the behavior of high-resistivity dielectrics in space radiation environments and is currently developing new methods for deriving dielectric resistivity.*

10. ACKNOWLEDGMENTS

The research described in this paper was carried out at the Jet Propulsion Laboratory, California Institute of Technology, under a contract with the National Aeronautics and Space Administration.